Automatic Modeling and Classification of Vitreomacular Traction Pathology Stages

Agnieszka Stankiewicz[1], Tomasz Marciniak[1], Adam Dąbrowski[1],
Marcin Stopa[2,3], Piotr Rakowicz[2,3], Elżbieta Marciniak[2]

[1] Division of Signal Processing and Electronic Systems
Chair of Control and Systems Engineering
Faculty of Computing
Poznan University of Technology
Poznan, Poland
e-mail: tomasz.marciniak@put.poznan.pl

[2] Clinical Eye Unit and Pediatric Ophthalmology Service, Heliodor Swiecicki University Hospital,
Poznan University of Medical Sciences
Poznan, Poland

[3] Department of Optometry and Biology of Visual System,
Poznan University of Medical Sciences
Poznan, Poland
e-mail: stopa@ump.edu.pl

***Abstract*—Retinal pathologies that are detected too late and/or left untreated can seriously damage eyesight. It is important to monitor the retina and react to any pathological changes. A fast, accurate, non-invasive, and even three-dimensional retina examination is the optical coherence tomography (OCT). In this paper we propose a new automated classification method for evaluation of vitreomacular interface (VRI) in human eyes. We present an approach for modelling changes in retina structure during the progression of vitreomacular traction (VMT) pathology. Presented experiments were performed on volumetric data acquired from adult patients with the use of Avanti RTvue device. Advanced digital image processing algorithms were subsequently applied to each OCT cross-section (B-scan) for image denoising and flattening, as well as retina layers segmentation. The proposed solution has a good accuracy and almost all subjects were successfully classified into one of 4 groups corresponding to various stages of VMT. The developed models of VMT stages show a high potential of the proposed method to support ophthalmologists in making appropriate clinical decisions.**

***Keywords*—OCT, vitreoretinal interface, pathology detection, retina modelling, medical image processing.**

I. Introduction

The largest structure within the human eye is the vitreous body. Since birth it is fully attached to the retina. Normal vitreoretinal physiology defines the interface between the vitreous and the retina (vitreoretinal interface, VRI), as a complex structure that undergoes natural age-related changes. A very important one is the liquefaction and detachment of the vitreous from the retina (posterior vitreous detachment, PVD) [1]. This process, mostly asymptomatic and nonpathologic, usually begins in the macula, and takes several months or years until full detachment [2]. Studies have shown that PVD occurs in around 50% adults at ages 30–39 years, and almost all the subjects aged 80 years or older, and is significantly more common with women than men [3].

Persistent attachment of vitreous in early VRI separation is described as vitreomacular adhesion (VMA) and characterized with no detectable changes in underlying retinal tissues [4]. It can spontaneously resolve into full detachment or cause incomplete and anomalous PVD. Subsequent possible stages of anomalous PVD are illustrated in Fig. 1.

Strong adherence during the progression of PVD can cause excessive traction on the macula, and results in anatomic changes of the fovea (such as cysts or elevation of layers) causing reduced or distorted vision [5]. An elevation of retinal surface by traction forces and a distortion of the intraretinal structure is called vitreomacular traction (VMT) and is a subject for surgical therapy [6].

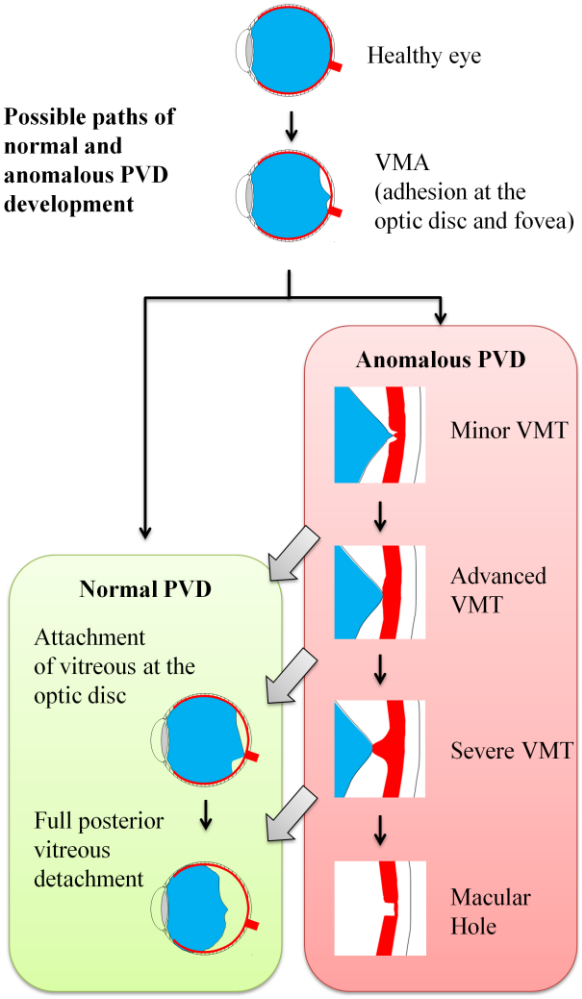

Fig. 1 Possible path of PVD evolution

During the evolution of VMT pathology the natural reversion to the healthy status is possible. Although if left untreated, the probability of developing a macular hole and severe retina damage increases with time. The risk of developing the same condition on the patient's fellow eye is still unknown. Thus, it is important to monitor the changes in the macula over time, as such monitoring provides valuable information in making clinical healthcare decisions, as well as after surgery control [7].

The optical coherence tomography (OCT) is a valuable tool aiding the evaluation of retinal thickness, as it provides quantitative assessment of retinal layers with noninvasive measurement technology [8]. This pertains also to the investigation of the vitreoretinal interface [9]. The volumetric OCT scans provide information of the retinal layers as well as the topography of the retina. Various stages of normal and anomalous PVD detachment acquired with OCT technology are illustrated using single B-scan (cross-section) in Fig. 2 (arrows indicate places of detachment).

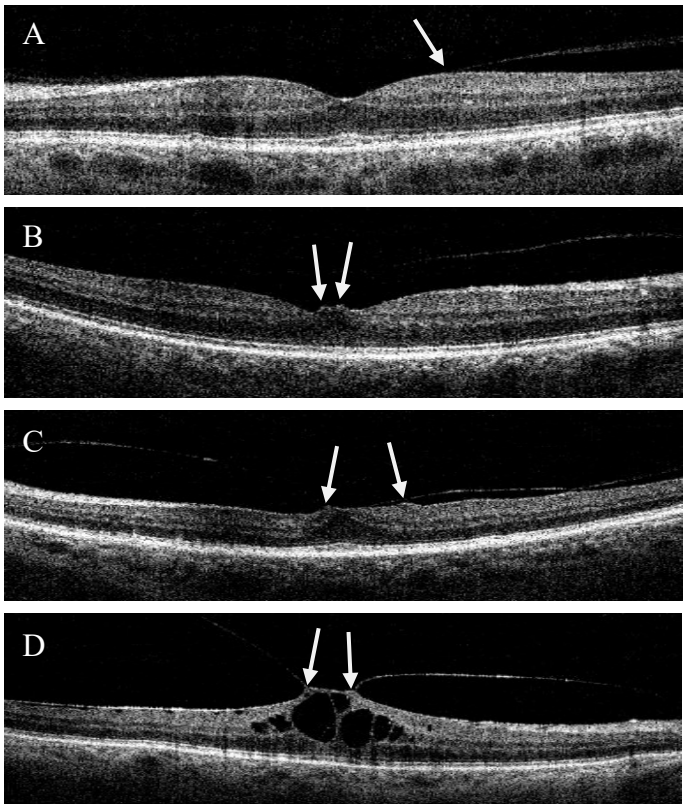

Fig. 2. Various stages of anomalous PVD development with annotated points of adhesion/traction: A: VMA; B: early VMT – traction in the fovea region; C: moderate VMT - distortion of retinal layers; D: severe VMT – rupture of intraretinal structure

The understanding of VMT creation is still insufficient, and a detailed analysis of distribution of traction forces during this process would be beneficial to the doctors' community. A valuable tool for visualizing VMT are virtual maps representing distances between posterior vitreous cortex and surface of the retina [10, 11]. The newest research characterizing VMT development suggest retina shape and its depth at the fovea as significant parameters describing VMT advancement [12]. Since the classification of vitreomacular interface changes is a relatively unexploited area of research, no one to the best of our knowledge attempted the problem of automated modeling the VMT pathology development.

Our previous study showed that analysis of retinal layers for a single OCT cross-section has a potential for classification of various intraretinal pathologic changes [13]. Nevertheless, since VMA is most likely to start in the superior part of the macula (probably due to gravitational forces) [14], it is not certain that the VMT pathology will begin in the fovea pit. Thus, a detailed 3D visualization would be better than a single cross-section analysis in this type of application.

In this report we try to establish, if the topographic map of the macular region embeds enough information to assess the progression of the VMT pathology. We aim to take advantage of pattern recognition algorithms and help in establishing an automatic approach for determining the risk of developing VMT pathology for clinicians.

The proposed solution should evaluate what is the current state of PVD development and what are the chances of improper VRI segmentation, as well as what is the most probable path of pathology progression for a given patient. Such computer-aided diagnostic tool would be very beneficial in drawing specialist's attention to possible abnormalities and indicating possible treatment courses.

II. OCT RETINA THICKNESS MAPPING

Retina atlas construction for medical purposes has been a research field of its own [15]. In this application, we propose a simplified mathematical model of retina topography that is further expanded to mimic the stages of VMT progression.

The model description is based on volumetric OCT macular scans of several healthy patients. Analysis of the gathered data in form of a three-dimensional block aids in the morphology investigation. For each scan a segmentation of the inner limiting membrane (ILM) and the upper interface of the retinal pigment epithelium (RPE) were performed (Fig. 3). Algorithm used for the segmentation of retinal layers was developed by [16] and further improved to account for low quality of OCT scans and discontinuities caused by VMT [10, 17]. This segmentation allows for establishing the topography of VRI with respect to the depth of the retina tissue, as is illustrated on Fig. 4.

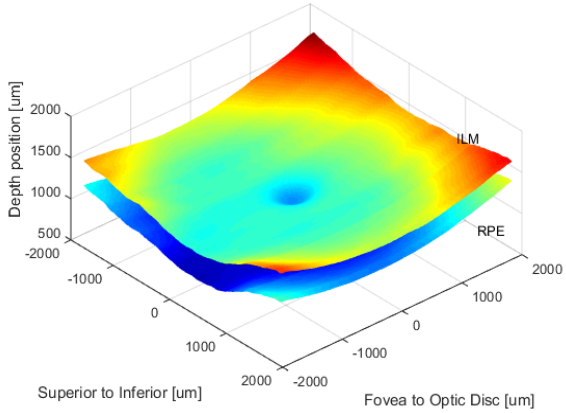

Fig. 3. Segmented ILM and RPE layers

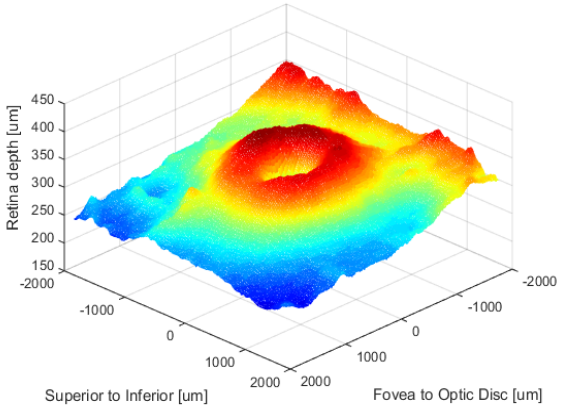

Fig. 4. Resulting topographic map of the retina

Rendering accurate visualization of 3D retina map involves also flipping the data for left eyes (from left to right), so that the topology of both eyes can be compared, and all scans can represent a unified human retina atlas (RT-Atlas).

As the standard OCT examination provides volumetric data representing tissue of 7×7 mm or more, and the diagnostic procedures examine the central portion of this area, a selection of the macular region of 4×4 mm is done. This is performed, based on the knowledge of our previous research [13], as well as an analysis of other reports [18].

During this step we aim to ensure that all the maps have the origin of coordinate system in the center of fovea depression, what aims to correct for eye shift and rotation. Additionally, thanks to this procedure, values in the horizontal axis correspond to the nasal (positive values) and temporal (negative values) part of the macula, with respect to the fovea. Similarly, the vertical axis describes areas belonging to the superior (negative values) and inferior (positive values) macula. The fovea center for the disrupted tissue was assessed by ophthalmology experts after OCT examination.

The volumetric OCT examination is represented by a collection of cross-sections, for which the width of each B-scan has much higher resolution than the number of B-scans [19]. This means that the resolution of a 3D scan is nonuniform with respect to the examined tissue. To ensure the uniform distribution of the data in the RT-Atlas we increased the accuracy of created maps to subpixel precision by bicubic interpolation.

III. VMT STAGES MODELING

A. Definition of VMT stages

Based on the findings provided by the International Vitreomacular Traction Study Group [4], we know that to classify an eye as having VMT, the following criteria must be fulfilled on at least one OCT B-scan:

- vitreous cortex detachment from the retinal surface
- vitreous cortex attachment within a 3-mm radius from the fovea
- distortions in fovea surface or changes in intraretinal structure.

Apart from that, both VMA and VMT can be further subclassified as focal or broad, depending on the width of vitreous attachment. Unfortunately, sometimes VMT is hard to distinguish from focal VMA, due to only subtle distortion of the fovea contour [6]. Such slight elevation of fovea margins may be difficult to detect, especially during simplified OCT examination.

The latest research regarding VMT stages analysis suggests retina shape classification into three phases: normal shape of healthy retina, distortion of inner retina at the fovea, and eversion of retina [12]. Careful analysis of many OCT cross-sections with various degrees of VMT development allowed us to introduce one additional VMT stage, as described in Table 1. Corresponding B-scans for selected stages are presented in Fig. 2.

It should be noted, that the proposed definitions succumb to further improvement as our knowledge of vitreoretinal diseases and their underlying pathophysiologic characteristics advances.

B. Model description

In the literature several papers on pathology modeling and identification can be found. They describe attempts of automated macular pathology diagnosis for macular edema [20], macular hole [21], and age-related macular degeneration [22]. Most of them try to establish the possibility of finding abnormalities based on the analysis of 2D slices from the macular OCT volume [23].

Table 1. Classification of VMT stages

Stage	Name	Description
0	VMA	vitreous cortex detachment from the retinal surface, no distortion of retinal tissue
1	early VMT	vitreous cortex attachment at the foveal pit, subtle distortion of the foveal contour, no disruption of intraretinal layers
2	moderate VMT	central portion of retinal layers elevated by traction forces to the upper level of ILM
3	severe VMT	rupture of intraretinal structure with intraretinal cysts or macular hole caused by traction

Computational methods used for this purpose are mainly local binary pattern histograms, mean squared error for fitting a mathematical model [18] or statistical analysis of segmented OCT images [24]. Support vector machines (SVM) [20, 21], logistic regression or artificial neural network [22] are the most common choices for data classification.

Nevertheless, the characteristics of VMT induced the selection of a 3D model for pathology investigation. This is motivated by the fact that a volumetric data representation contains more relevant information about changes distribution, as was confirmed by recent research reports [12].

For the model creation we selected a set of 3D OCT scans for each group of previously defined VMT stages. Based on our assumption, that the information about pathology distribution and its size can be extracted from retina layers' shape, we computed a retina map for each examination in the set as described in section II.

To specify a 3D model of each VMT phase we utilized a mean squared error minimization algorithm to find the best fit of a surface representing all of the topographic maps obtained from the OCT examinations (one surface map for one VMT stage). This way, for each map coordinate of x and y we get surface $S(x, y)$.

In the next step, the obtained surface is modeled with a thin-plate spline interpolation in order to estimate a smooth representation of the characteristic shape of retina for every stage. In our application this means minimization of the following function by the smoothing spline $f(x, y)$[25]:

$$\min_f \; pE(f(x,y)) + (1-p)R(f(x,y)) \tag{1}$$

In the weighted sum (1) $E(f(x,y))$ specifies the error measure that can be calculated for a given set of $M \times N$ corresponding points as:

$$E(f(x,y)) = \sum_{i=1}^{M}\sum_{j=1}^{N} \left\| S(x_{ij}, y_{ij}) - f(x_{ij}, y_{ij}) \right\|^2 \tag{2}$$

The second function $R(f)$ represents the roughness measure that can be used to relax the requirement of interpolant passing exactly through the data points:

$$R(f(x,y)) = \iint \left(\left(\frac{\partial^2 f(x,y)}{\partial x^2} \right)^2 + 2\left(\frac{\partial^2 f(x,y)}{\partial x \partial y} \right)^2 + \left(\frac{\partial^2 f(x,y)}{\partial y^2} \right)^2 \right) \mathrm{dxdy} \tag{3}$$

The smoothing parameter p defines, if the smoothing spline will represent the least-squares approximation to the data (when $p = 0$), or a thin-plate spline (for $p = 1$). In the proposed solution we chose p value close to 1. This approach allows defining a smooth surface that adequately represents desired distorted retina shape.

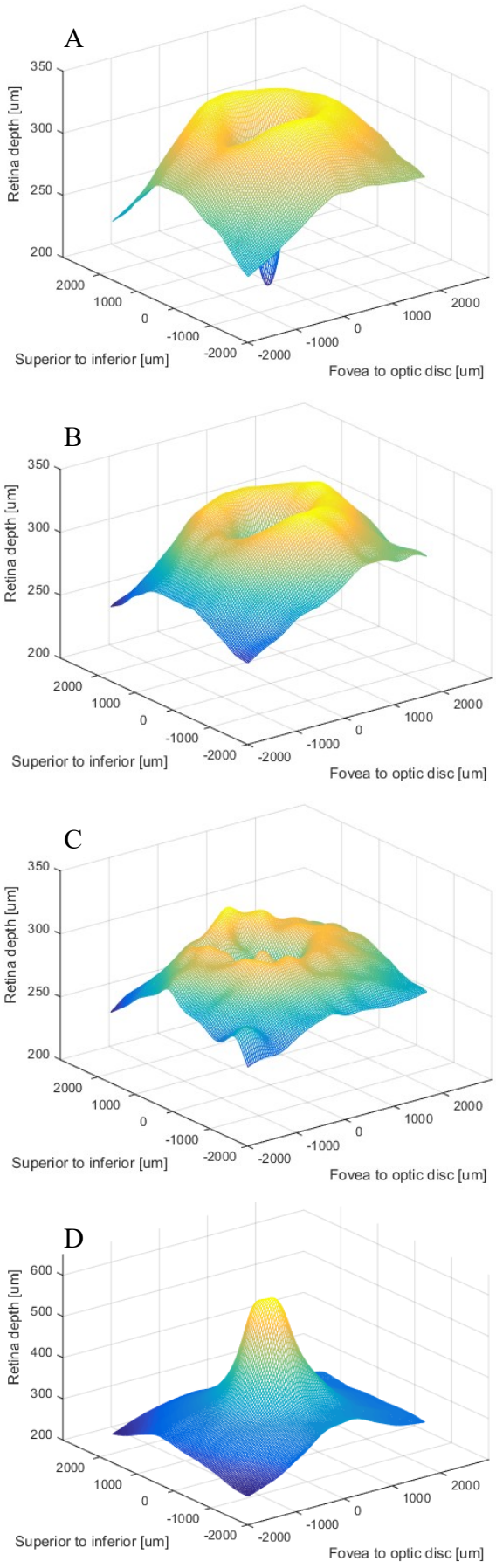

Fig. 5. Fovea models for VMT stages
(A: stage 0, B: stage 1, C: stage 2, D: stage 3)

The thin-plate spline interpolation has been chosen for shape matching, because it produces a smooth surface and has a physical explanation of its energy function [26]. Additionally, it does not require manual tuning of parameters.

Figure 6 shows the computed 3D models for all VMT stages. Constructed surface has the origin of the coordinate system located at the center of the fovea, and the values on the vertical axis corresponds to the retinal thickness.

Careful analysis of the obtained models clearly shows distinguishable differences between them. The first model (A) represents a proper model of a healthy retina with the asymmetric depression on the temporal side and a characteristic deep pit in the central point. This fovea depression is less distinguished in Model B as the ILM layer is slightly elevated. Additionally, the surface shape around the depression has irregularities. These distortions are even more apparent in the third model (C), while the central depression is further elevated. As was expected, the last model (D) shows the most distinct characteristic of a total elevation of ILM layer in the fovea region.

IV. Classification tests

A. Database

To perform the classification tests we composed a database of 3D OCT scans acquired with the use of Avanti RTvue device. 15 patients with various stages of VMT development (5 in each stage) and 5 healthy volunteers were carefully selected for the study. The database consists of 12 right and 8 left eyes from 12 women and 8 men of average age of 65, 72, 71 and 76 years for stages 0 to 3 respectively. All of the patients gave their informed consent before the enrollment. The proposed study was approved by the local institutional ethical board.

For each patient a full OCT examination was performed and a 7×7 mm macula scan was obtained. Each scan consists of 141×385×640 data points (141 B-scans of 385×640 image resolution) from which a retina map of 385×385 points was calculated in Matlab/Simulink environment. This map was further cropped to the fovea region (4×4 mm) represented by 220×220 points. From such topographic map a model of the same size was calculated.

Unfortunately, due to computational issues we were forced to reduce the model size by half (to 110×110 points) with bicubic interpolation. For the investigational purposes we also tested a model reduced 4 times (to 55×55 points). In the next step each model was unfolded into a vector of the length equal to the number of data points. Such prepared data was later used as a feature vector d .

B. Classification algorithm

For the classification task we selected a support vector machines (SVM) method implemented in Python programming language with the use of *scikit-learn* library [27]. The multi-class supervised learning algorithm utilized an one-vs-rest modeling approach. As a kernel function we chose two types of functions linear and radial basis function (RBF).

For the SVM classification algorithm the penalty weight C (that controls the separability margin of the decision hyperplane) needs to be determined. We experimentally chose this value to be equal to 10000 using the training data set. The parameter r was set to 0, and the optimal value of the α parameter varied from 10^{-7} for the model size of ½ to 10^{-9} for ¼ of the model resolution, and was also chosen experimentally using the training data set.

Due to the fact, that the gathered dataset is relatively small, we assessed the performance of the SVM system by 5-fold cross-

validation. This means, that the dataset was divided into 5 parts, from which 4 were used for model creation, and one was used for testing. This was repeated 5 times, leaving out a different scan each time.

V. Results

In this section we present results of the VMT stages classification algorithm. Values of precision, recall and F1-score for each conducted test are included in Tables 2-5. As can be expected the best results were obtained for RBF classifier and a model of ½ of its original size.

The general accuracy for linear classifier was 85% for model of the size ½, and 80% for ¼ of the model. Slightly better results produced the RBF kernel giving the accuracy of 90% and 85% for ½ and ¼ of the model sizes respectively.

Table 2. Classification results for linear classifier (model size: ½)

Stage	Precision	Recall	F1-score
0	1.00	1.00	1.00
1	0.80	0.80	0.80
2	0.71	1.00	0.83
3	1.00	0.60	0.75
Average	0.88	0.85	0.85

Table 3. Classification results for linear classifier (model size: ¼).

Stage	Precision	Recall	F1-score
0	1.00	1.00	1.00
1	0.80	0.80	0.80
2	0.62	1.00	0.77
3	1.00	0.40	0.57
Average	0.86	0.80	0.79

Table 4. Classification results for RBF classifier (model size: ½).

Stage	Precision	Recall	F1-score
0	1.00	1.00	1.00
1	0.80	0.80	0.80
2	0.80	0.80	0.80
3	1.00	1.00	1.00
Average	0.90	0.90	0.90

Table 5. Classification results for RBF classifier (model size: ¼).

Stage	Precision	Recall	F1-score
0	1.00	1.00	1.00
1	1.00	0.80	0.89
2	0.62	1.00	0.77
3	1.00	0.60	0.75
Average	0.91	0.85	0.85

What can clearly be discerned from the obtained results is that, the distinct shape of the third stage (severe VMT) is easily detected by the classification algorithm, as well as the healthy macula (VMA). The first (early VMT) and second (moderate VMT) models are similar, hence the misclassifications between them. Nevertheless, although differences between healthy retina and early stage of VMT cannot always be perceived by visual inspection (sometimes it requires a detailed analysis), this first pathological step is clearly distinguishable by the proposed application. This suggests that the mapping technique is useful in assessment of retina in the initial stage of VMT.

Figure 6 illustrates a confusion matrix for the best obtained result (RBF classifier with ½ of the model) and in Fig. 7 ROC (receiver operating characteristic) curves for conducted tests are depicted.

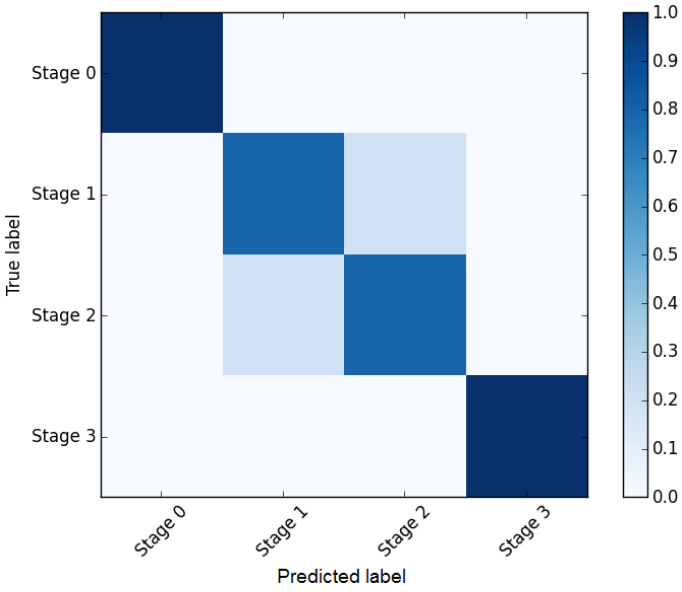

Fig. 6. Confusion matrix for RBF classifier (model size: ½)

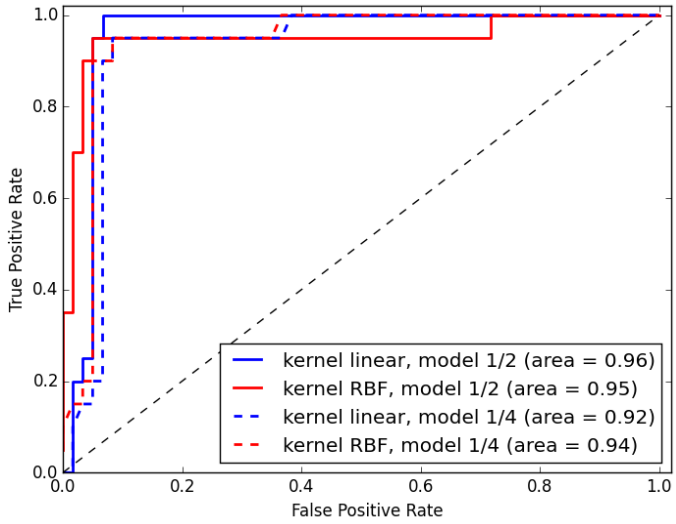

Fig. 7. ROC curves for each classifier

VI. Concluding Remarks

The presented research addresses a problem of automatic evaluation of VMT pathology development. The conducted experiments confirmed a possibility of correct automatic recognition of various VMT stages. This identification is based on the topographic maps of human retina. All of this relies on the assumption that traction forces have impact on the retinal shape. We proposed a set of models of the macular topography calculated with the use of thin-plate smoothing spline. It would be prudent to introduce a more detailed classification of VMT stages and models representing transitional steps between them.

The suggested algorithm utilizing SVM classification method with RBF kernel has good accuracy. The system performance can be significantly fastened by reducing the size of model, while retaining acceptable sensitivity. It should be noted that the low number of data examples being a drawback in this experiment will be systematically expanded as the database of patients with VRI pathologies will grow concurrently with the project realization. Further experiments should also evaluate the influence of data standardization on the proposed as well as other modeling technique.

The real challenge brought before the clinicians is to determine how the changes of the retina structure will unfold, based on actual pathology model. This is a very difficult and important task, as the adhesion sights can at any time resolve into normal PVD, or will require surgical intervention. This divides the VMT development into many various paths.

ACKNOWLEDGMENT

This work was prepared within the Project REVEMOD number 09/93/DSMK/1602.

REFERENCES

[1] D. Steel and A. Lotery, Idiopathic vitreomacular traction and macular hole: a comprehensive review of pathophysiology, diagnosis, and treatment, *Eye*, *27*: 1–21, 2013.

[2] E. Uchino, A. Uemura, and N. Ohba, Initial stages of posterior vitreous detachment in healthy eyes of older persons evaluated by optical coherence tomography, *Arch Ophthalmol*, *119*: 1475–9, 2001.

[3] J. Sebag, Age-related changes in human vitreous structure., *Graefes Arch Clin Exp Ophthalmol*, *225*: 89–93, 1987.

[4] J. S. Duker, P. K. Kaiser, S. Binder, et al., The International Vitreomacular Traction Study Group classification of vitreomacular adhesion, traction, and macular hole, *Ophthalmology*, *120(12)*: 2611–2619, 2013.

[5] M. W. Johnson, Posterior vitreous detachment: evolution and role in macular disease, *Retina*, *32:* 174–178, 2012.

[6] P. Stalmans, J. S. Duker, P. K. Kaiser, et al., OCT-based interpretation of the vitreomacular interface and indications for pharmacologic vitreolysis, *Retina*, *33(10)*: 2003–2011, 2013.

[7] M. W. Johnson, Perifoveal vitreous detachment and its macular complications, *Trans Am Ophthalmol Soc*, *103*: 537–67, 2005.

[8] M. A. Baroni, P. B. Fortunato, and A. La Torre, Towards Quantitative Analysis Of Retinal Features In Optical Coherence Tomography, *IPEM, Elsevier*, 2006.

[9] M. Codenotti, L. Iuliano, G. Fogliato, and et al., A novel spectral-domain optical coherence tomography model to estimate changes in vitreomacular traction syndrome, *Graefes Arch Clin Exp Ophthalmol*, 2014.

[10] A. Stankiewicz, T. Marciniak, A. Dabrowski, M. Stopa, and E. Marciniak, A New OCT-based Method to Generate Virtual Maps of Vitreomacular Interface Pathologies, *Proceedings of 18th IEEE International Conference on Signal Processing (SPA 2014)*, 83–88, 2014.

[11] R. Malagola, N. Iozzo, and P. Grenga, Volumetric assessment of the space between the posterior hyaloid and internal limiting membrane using SD-OCT, *Br J Ophthalmol*, *98*: 16–18, 2014.

[12] D. H. Steel, L. Downey, K. Greiner, et al., The design and validation of an optical coherence tomography-based classification system for focal vitreomacular traction, *Eye*, *30(2)*: 314–24, 2016.

[13] A. Stankiewicz, T. Marciniak, A. Dąbrowski, M. Stopa, P. Rakowicz, and E. Marciniak, Automatic identification of macular pathologies in OCT retina images using SVM-based approach, in *IFIP Doctoral Seminar on Software-Intensive Systems Engineering*, 2015.

[14] M. Stopa, E. Marciniak, P. Rakowicz, A. Stankiewicz, T. Marciniak, and A. Dąbrowski, Imaging and measurement of the preretinal space in vitreomacular adhesion and vitreomacular traction by a new SD-OCT scan analysis, in *XLVII Polish Ophthalomogists Convention, Retina - diagnosis*, 2016.

[15] G. Heitz, T. Rohlfing, and C. J. Maurer, Statistical shape model generation using nonrigid deformation of a template mesh, *Medical Imaging 2005: Image Processing*, *5747*: 1411–1421, 2005.

[16] S. J. Chiu, X. T. Li, P. Nicholas, et al., Automatic segmentation of seven retinal layers in SDOCT images congruent with expert manual segmentation, *Optics express*, *18(18)*: 19413–19428, 2010.

[17] A. Stankiewicz, T. Marciniak, A. Dąbrowski, P. M. Rakowicz Stopa, and E. Marciniak, Improving Segmentation of 3D Retina Layers Based on Graph Theory Approach for Low Quality OCT Images, *Metrology and Measurement Systems*, *23(2)*: 269–280, 2015.

[18] R. Bernardes, T. Santos, and J. Cunha-Vaz, Increased-Resolution OCT Thickness Mapping of the Human Macula: A Statistically Based Registration, *Investigative Ophthalmology & Visual Science*, *49(5)*: 2046–2052, May 2008.

[19] Optovue and Inc., *RTVue XR 100 Avanti Edition. User manual*. 2014.

[20] Y.-Y. Liu, M. Chen, H. Ishikawa, et al., Automated macular pathology diagnosis in retinal OCT images using multi-scale spatial pyramid and local binary patterns in texture and shape encoding, *Medical image analysis*, *15(5)*: 748–759, 2011.

[21] A. S. C. Silva, J. Figueira, S. Simao, et al., Unveiling preclinical idiopathic macular hole formation using support vector machines, in *Biomedical and Health Informatics (BHI), 2014 IEEE-EMBS International Conference on*, 2014, 585–588.

[22] S. Krishnaiah, B. R. Surampudi, and J. Keeffe, Modeling the risk of age-related macular degeneration and its predictive comparisons in a population in South India, *International Journal of Community Medicine and Public Health*, *2(2)*: 137–148, May 2015.

[23] Y. Jiang, K. Mazittello, M. Chrenek, et al., Modeling Morphology Dynamics of Retinal Pigment Epithelium.

[24] T. Santos, L. Ribeiro, C. Lobo, et al., Validation of the Automatic Identification of Eyes with Diabetic Retinopathy by OCT, in *IEEE 2nd Portuguese Meeting in Bioengineering (ENBENG)*, 1–4, 2012.

[25] J. Mitra, R. Mart, A. Oliver, et al., A Comparison of Thin-plate Splines with Automatic Correspondences and B-splines with Uniform Grids for Multimodal Prostate Registration, in *Proc. of SPIE Medical Imaging 2011: Visualization, Image-Guided Procedures, and Modeling*, 2011, *7964*.

[26] F. L. Bookstein, Principal warps: thin-plate splines and the decomposition of deformations, *IEEE Transactions on Pattern Analysis and Machine Intelligence*, *11(6)*: 567–585, Jun. 1989.

[27] F. Pedregosa, G. Varoquaux, A. Gramfort, et al., Scikit-learn: Machine Learning in Python, *Journal of Machine Learning Research*, *12*: 2825–2830, 2011.